International Journal of Biological Macromolecules 333 (2025) 148860

Contents lists available at ScienceDirect

International Journal of Biological Macromolecules

journal homepage: www.elsevier.com/locate/ijbiomac

A π-stacking gate for redox control in flavin ferredoxin-thioredoxin reductases

Martha Minjarez-Saenz [a], Víctor Correa-Pérez [a], Maribel Rivero [a], Sheila J. Sadeghi [b], Javier Calvo [c], Adrián Velázquez-Campoy [a], Federico Gago [d], Rubén M. Buey [e], Marta Martínez-Júlvez [a], Milagros Medina [a,*], Monica Balsera [c,*]

[a] Department of Biochemistry and Molecular and Cellular Biology, Faculty of Sciences and Institute for Biocomputation and Physics of Complex Systems (BIFI), University of Zaragoza, 50009, Zaragoza, Spain
[b] Department of Life Sciences and Systems Biology, University of Torino, Italy
[c] Department of Abiotic Stress, Institute of Natural Resources and Agrobiology of Salamanca (IRNASA-CSIC), 37008, Salamanca, Spain
[d] Department of Biomedical Sciences, School of Medicine and Health Sciences, University of Alcalá, Alcalá de Henares, Spain
[e] Metabolic Engineering Group, Department of Microbiology and Genetics, Faculty of Biology, University of Salamanca, Unit associated to CSIC through IRNASA, 37007, Salamanca, Spain

ARTICLE INFO

Keywords:
Flavoenzymes
Redox disulfide
Electron transfer

ABSTRACT

Flavin ferredoxin-thioredoxin reductases (FFTRs) constitute a unique class of enzymes that transfer electrons from low-potential ferredoxins (Fdxs) to thioredoxins (Trxs) through a flavin cofactor. They are widely distributed across bacterial lineages, including cyanobacteria and anaerobes such as Clostridium, where they function either as the sole Trx reductase or in parallel with canonical NADPH-dependent or iron–sulfur systems. A distinguishing feature of cyanobacterial FFTRs is a C-terminal tail containing a conserved tryptophan (Trp) that engages in a π-stacking interaction with the flavin—a motif absent in clostridial orthologs. In this study, we use the cyanobacterial FFTR from *Gloeobacter violaceus* as a model to demonstrate that the C-terminal tail and its conserved aromatic residue modulate the FAD electronic environment, electron transfer efficiency, and Fdx donor interactions. Mutants lacking the tail or Trp exhibited increased flavin solvent exposure, a redox potential shift of over 200 mV toward less negative values, altered reduction kinetics, impaired electron flow to the redox-active disulfide, and reduced specificity for Fdx binding. These results reveal a dual role for the C-terminal tail: it establishes a productive donor-binding interface and shapes the FAD environment to meet the thermodynamic and kinetic requirements for efficient intramolecular electron transfer to the redox-active disulfide. Collectively, these findings provide mechanistic insight into how peripheral structural features, such as FAD-aromatic π-stacking interactions, govern flavin reactivity, donor specificity, and redox behavior in cyanobacterial FFTRs, underscoring their relevance and offering a framework for engineering redox-active biocatalysts for synthetic biology and metabolic applications.

1. Introduction

Thioredoxin (Trx) systems are essential for maintaining redox homeostasis and regulating protein thiol-disulfide exchange reactions in response to environmental and metabolic cues [1–3]. In most organisms, Trx reduction is mediated by either flavin NADPH-dependent thioredoxin reductases (NTRs) or iron–sulfur ferredoxin-thioredoxin reductases (FTRs). However, a subset of phylogenetically diverse organisms—including the cyanobacteria *Gloeobacter*, *Prochlorococcus*, and *Synechococcus*, as well as certain *Clostridium* species—lack both NTRs and FTRs; consequently, they rely exclusively on flavin ferredoxin-thioredoxin reductases (FFTRs) to sustain Trx-dependent redox regulation [4,5]. The finding that, in other bacteria and algae, FFTRs coexist with NTRs or FTRs suggests that FFTRs may complement or specialize redox regulation under specific physiological or stress conditions [6].

FFTRs catalyze electron transfer (ET) from reduced ferredoxin (Fdx)

Abbreviations: CTC, charge transfer complex; FFTR, Ferredoxin-Dependent Flavin Thioredoxin Reductase; NTR, NADPH-dependent Thioredoxin Reductase; ox, oxidized; hq, hydroquinone; sq, semiquinone; Trx, Thioredoxin; DTH, Dithionite; Fdx, ferredoxin; 5-dRf, 5-deazariboflavin.

* Corresponding authors.
E-mail addresses: mmedina@unizar.es (M. Medina), monica.balsera@csic.es (M. Balsera).

https://doi.org/10.1016/j.ijbiomac.2025.148860
Received 1 October 2025; Received in revised form 3 November 2025; Accepted 5 November 2025
Available online 6 November 2025

to Trx, directly linking photosynthetic or fermentative electron flow to downstream redox processes [4,5]. In marine cyanobacteria such as *Prochlorococcus*, FFTR activity is thought to be tightly coupled to photosynthetic Fdx, enabling light-dependent regulation of primary metabolism in phytoplankton. In anaerobic bacteria like *Clostridium difficile,* FFTRs are implicated in sporulation and fermentation, processes critical for survival, dissemination, and industrial biotechnology [7]. The presence of FFTR as the sole Trx reductase in some of these organisms underscores its physiological relevance and positions it as a key player in redox regulation across diverse metabolic contexts.

FFTRs are homodimeric flavoproteins structurally related to low-molecular weight NTRs (LMW-NTRs), but they use Fdx instead of pyridine nucleotide as the electron donor [6,8,9]. Despite their shared architecture, FFTRs and LMW-NTRs exhibit distinct mechanistic and structural features [5,10]. In the homodimer, each protomer contains two domains: a FAD-binding domain with a non-covalently bound FAD and a second domain that harbors a CxxC motif, referred to as the redox-active disulfide domain in FFTRs or the NADPH-binding domain in NTRs [5,6]. Similar to NTRs, the catalytic mechanism in FFTR involves sequential ET from the electron donor to FAD (flavin reductive half-reaction), then from reduced FAD to the internal disulfide (flavin oxidative half-reaction), and finally from the reduced dithiol to Trx. These steps are coordinated by conformational dynamics that govern ET timing and directionality [5,11].

FFTRs appear to have diverged structurally and functionally to accommodate different redox environments. Whereas clostridial FFTRs interact with bacterial-type [4Fe—4S] Fdxs capable of two-ET, cyanobacterial FFTRs use plant-type [2Fe—2S] Fdxs that operate via sequential single-ET [4,5,11,12]. A key structural distinction is the presence of a C-terminal tail in the cyanobacterial enzymes, which includes a conserved aromatic residue. This residue forms a π-stacking interaction with the FAD isoalloxazine ring of the adjacent protomer (Fig. 1A) [5,6]. Aromatic–flavin π-interactions are known to modulate redox properties in other flavoproteins, such as ferredoxin-NADP$^+$ reductases (FNRs), flavodoxins (Flvs) and cytochrome P450 oxidoreductases [13–17]. For example, mutation of Tyr303 in *Anabaena* FNR alters

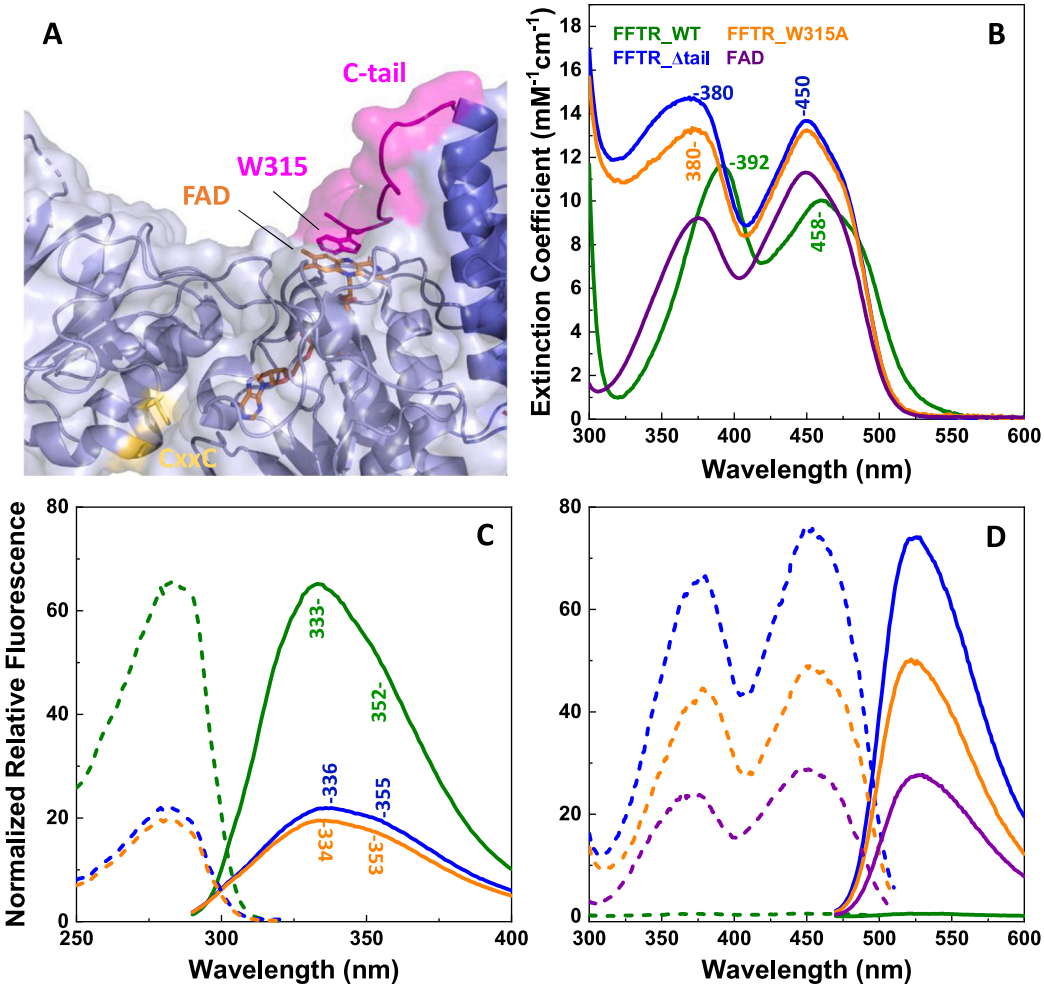

Fig. 1. Structural features and spectroscopic properties of *G. violaceus* FFTR C-terminal tail variants. A Close-up view of the FAD active site in the crystal structure of the *G. violaceus* FFTR homodimer (open conformation PDB code 5J60). The two protomers are shown as cartoon with transparent surface, one colored in light-blue and the other in dark-blue. Only the FAD cofactor of the light-blue protomer is displayed (sticks, carbons in orange). The CxxC motif of this protomer is highlighted in yellow (side chains in sticks). From the neighboring dark-blue protomer, the C-terminal tail (Ser307-His317) is shown, with Trp315 in sticks (carbons in magenta) stacking against the re face of the FAD. B Visible absorption spectra, C far UV fluorescence spectra, and D visible fluorescence spectra of FFTR_WTox (green), FFTR_Δtailox (blue) and FFTR_W315Aox (orange). Solid lines show the fluorescence emission spectra upon excitation at 280 nm and 600 V in C and 460 nm and 700 V in D, while dashed lines correspond to excitation spectra when collecting fluorescence at 333 nm in C and 527 nm in D. Panels B and D also include the spectrum of free FADox (violet). Spectra were recorded in 10 mM potassium phosphate, pH 8.0, at 25 °C. Fluorescence spectra were normalized to the corresponding protein concentration determined from the extinction coefficient at the flavin band I. All samples were measured at identical protein concentrations under the same buffer conditions. Relevant spectral peaks are highlighted in B and D. Data correspond to a representative experiment ($n = 3$). (For interpretation of the references to colour in this figure legend, the reader is referred to the web version of this article.)

the redox potential and affects hydride transfer efficiency, highlighting the role of aromatic side chains in tuning flavin chemistry [15,18]. These precedents underscore the importance of aromatic-stacking interactions in modulating redox properties and support the rationale for investigating π-stacking in FFTRs.

In this study, we employ the cyanobacterial FFTR from *G. violaceus* as a model to dissect the molecular determinants of flavin redox tuning and electron donor specificity. Through site-directed mutagenesis and chimeric protein constructs, combined with spectroscopy, redox titrations, and kinetic analyses, we elucidate how the C-terminal tail and its conserved aromatic residue modulate the FAD electronic environment and ET efficiency. Our results reveal a dual role for the C-terminal tail: it both establishes a productive donor-binding interface and shapes the FAD environment to satisfy the thermodynamic and kinetic requirements for efficient intramolecular ET. These findings provide mechanistic insight into how peripheral structural features, such as π-stacking interactions, govern flavin reactivity and redox behavior in FFTRs. This underscores their functional relevance in physiologically specialized systems.

2. Materials and methods

2.1. Protein expression and purification

Wild-type FFTR (FFTR_WT), the C-terminal deletion variant (FFTR_Δt) and Fdx1 from *G. violaceus*, as well as FFTR2 from *Clostridium acetobutylicum* were prepared as previously described [5,6,8]. Using the FFTR_WT expression vector as a template, a mutant enzyme was generated in which Trp315 was replaced by Ala (FFTR_W315A), aiming to disrupt the π-stacking interaction between the indole side chain of the Trp and the isoalloxazine ring of the flavin. A similar strategy was used to generate chimeric constructs in which the *fftr2* gene from *C. acetobutylicum* [8] and the *ntr* gene from *Escherichia coli* were each fused at their C-terminus to the C-terminal tail of *Gloeobacter* FFTR (residues 303–317), resulting in the chimeras CaFFTR2_Gvtail and EcNTR_Gvtail. Point mutations and insertions were prepared according to [19] and constructs were corroborated by DNA sequencing. Proteins were produced in Rosetta *E. coli* cells as N-terminal His-tag fusions containing a thrombin cleavage site. Soluble proteins were purified by Ni^{2+} affinity chromatography, followed by tag removal and gel filtration using a Sephacryl S-300 HR column (*Cytiva*) equilibrated in 20 mM Tris/HCl pH 7.6, 150 mM NaCl. Prior to gel filtration, flavoenzymes were incubated with excess FAD to ensure full saturation of the binding sites. Saturation was confirmed by comparing the FAD concentration with the protein concentration determined by the Bradford assay (*Bio-rad*), yielding a consistent 2:1 flavin-to-homodimer ratio. *Anabaena* FNR and Flv were prepared as described [20,21].

2.2. Spectroscopic analysis

UV–Visible absorption spectra were recorded at 25 °C using a Cary 3500 spectrophotometer (*Agilent Technologies*). The molar absorption coefficients for FFTR_WT (ε_{458nm} = 10.1 ± 1.3 mM^{-1} cm^{-1}) and FFTR_Δtail (ε_{450nm} = 13.9 ± 1.1 mM^{-1} cm^{-1}) were taken from [5]. The value for Fdx1 was assumed to be equivalent to that of *Anabaena* ferredoxin (ε_{423nm} = 9.4 mM^{-1} cm^{-1}), whereas the extinction coefficient for FFTR_W315A (ε_{450nm} = 13.1 ± 0.7 mM^{-1} cm^{-1}) was determined spectrophotometrically in this work by thermal denaturation for 10 min at 90 °C, followed by centrifugation, separation of the precipitated apoprotein, and spectroscopic quantification of the FAD released as previously described [22]. Herein these coefficients were used to determine protein concentration. Absorption spectra were recorded in 20 mM Tris/HCl pH 8.0, 150 mM NaCl. Excitation and emission fluorescence spectra were acquired using a Cary Eclipse fluorimeter (*Agilent Technologies*) at 25 °C in 10 mM potassium phosphate, pH 8.0, with homodimer protein concentrations in the 3–5 μM range.

Steady-state photoreduction of FFTR_W315A was carried out stepwise under anaerobic conditions by irradiation with a 150 W halogen lamp at room temperature for periods of up to 30 s in the presence of 4 μM 5-deazariboflavin (5-dRf) and 3 mM ethylenediaminetetraacetic acid (EDTA), following previously established protocols [5]. Anaerobic conditions were employed to prevent side reactions involving oxygen, in accordance with established protocols for studying flavoproteins that do not catalytically interact with it.

2.3. Determination of midpoint reduction potentials

Midpoint reduction potentials (E_m) of FAD for FFTR_Δt and FFTR_W315A were determined using two complementary procedures. The first one was the xanthine/xanthine oxidase (XO) method [24]. Reduction of FFTR by the xanthine/XO system [23,24] was carried out in a closed anaerobic cuvette with a final concentration of ~15 μM of FFTR, 1–2 mM xanthine, 5 μM of the methyl viologen (E_m = −446 mV, n = 1), 10 mM glucose and 10 U/mL glucose oxidase, in 20 mM Tris/HCl pH 8.0, 150 mM NaCl. Once anaerobic conditions were established using a Schlenk line, 7.8 μg/mL of bovine milk XO (Sigma-Aldrich) was added to the mixture, and spectra were recorded every 5 min for up to 2 h, scanning from 250 to 700 nm at 25 °C, in a CARY 3500 spectrophotometer (Agilent Technologies). Absorption changes accompanying reduction of the indicator dye (phenosafranine was used in the case of both FFTR mutants, E_m = −252 mV) and the flavoprotein at each point during the xanthine/XO reduction were used to determine the FFTR $E_{ox/hq}$ value using the Nernst equation as previously reported [11,23,24].

The second method for analyzing midpoint reduction potentials was cyclic voltammetry (CV). Measurements were carried out using an Autolab PGSTAT12 potentiostat controlled by the GPES3 software (*Ecochemie*, The Netherlands). The 1 mL glass electrochemical cell was equipped with a platinum wire counter electrode, an Ag/AgCl (3 M NaCl, E_m = +220 mV) reference electrode and a 3 mm diameter glassy carbon working electrode (*BASi*, USA). The glassy carbon electrode was modified with a mixture of the protein and poly (diallyldimethylammonium chloride) polymer (PDDA) as follows: 5 μL of PDDA was mixed with 5 μL of FFTR (130 μM) and drop coated onto the electrode [25]. The modified bioelectrode was stored overnight at 4 °C. The CV measurements were carried out at 25 °C under anaerobic conditions obtained by flushing the samples under a nitrogen saturated atmosphere. The potential was scanned between 200 and − 700 mV at a rate of 100 mV/s. Control experiments were carried out in the absence of the protein. Additionally, FAD was immobilized onto the electrode and subjected to scanning in the same manner as the protein solution. The supporting electrolyte was 50 mM KPi buffer, 100 mM KCl, pH 7.4.

2.4. Kinetic measurements by stopped-flow spectrophotometry of the FFTR FAD reductive half-reaction

The reduction of the FAD cofactor of FFTR was evaluated by fast kinetic stopped-flow spectrophotometry by using a SX.18MV spectrophotometer (*Applied Photophysics Ltd.*) interfaced with a photodiode array detector in the visible region according to established protocols [11,26]. Reduction kinetics were studied using as reductant either sodium dithionite (DTH) (final concentrations 5 mM), light irradiation from the instrument's source lamp, or the physiological electron donor in the form of photoreduced Fdx1 ($Fdx1_{rd}$). All samples were rendered anaerobic prior to loading into the stopped-flow system by subjecting them to several cycles of evacuation and bubbling with O_2-free argon, following usual procedures when studying redox processes involving flavoenzymes [26]. Samples were prepared in 20 mM Tris/HCl pH 8.0, 150 mM NaCl, at 25 °C, and supplemented with glucose (10 mM) and glucose oxidase (10 UI/mL) to maintain anoxic conditions. $Fdx1_{rd}$ samples were generated by photoreduction in the presence of 5-dRf/EDTA (4 μM/3 mM) [11,26]. To follow the kinetics of photoreduction within the stopped-flow chamber, anaerobic protein solutions, both in

the absence and in the presence of 5-dRf/EDTA (4 μM/3 mM), were mixed 1:1 with the same anaerobic buffer and exposed to photo-irradiation from the instrument's source lamp (150 W/CR OFR Xenon Short Arc Lamp, OSRAM). Fast mixing experiments were also performed under anaerobic conditions to evaluate ET from DTH or $Fdx1_{rd}$ to oxidized FFTR ($FFTR_{ox}$, FAD_{ox}) in 20 mM Tris/HCl pH 8.0, 150 mM NaCl, at 25 °C. Absorption data at multiple wavelengths in the 360–900 nm range were collected during the reaction using the Pro-Data-SX software (*App. Photo. Ltd.*) [26]. Typically, 400 absorption spectra across multiple wavelengths were collected during the selected measuring times. Reduction of $FFTR_{ox}$ by $Fdx1_{rd}$ was studied at molar ratios of homodimer FAD_{ox}:$Fdx1_{rd}$ of 1:1 and 1:4, with final homodimer $FFTR_{ox}$ concentrations ranging from 2.5 to 5 μM. Pro-Data-SX and Pro-Kineticist (*App. Photo. Ltd.*) were used to evaluate spectral evolution for the identified processes, as previously reported [26]. Nonetheless, in the specific system studied here, deconvolution analysis proved highly challenging, likely due to multiple overlapping conformational changes and redox processes contributing simultaneously to the observed spectroscopic changes over time [11,26]. This complexity precluded the reliable extraction of observed rate constants (k_{obs}) for individual steps (see Discussion).

2.5. Thioredoxin reductase activity assay

The Fdx-dependent reductase activity of FFTR mutants from *G. violaceus* was assessed by monitoring the reduction of 5,5′-dithiobis(2-nitrobenzoic acid) (DTNB) at 412 nm, following the protocol described by [27]. The reaction mixture contained 0.2 mM NADPH, 0.1 μM FNR from *Anabaena* [18], 2 μM Fdx1, 0.1 μM FFTR, 0.5 μM Trx-m and 0.5 mM DTNB. The NADPH-dependent reductase activity of EcNTR and the EcNTR_Gvtail chimera was evaluated using reaction mixtures containing 0.15 mM NADPH, 0.25 μM NTR and 0.25 mM DTNB. Reactions were carried out in 100 mM potassium phosphate buffer pH 7.0 containing 2 mM EDTA, at 25 °C. The Flv- and Fdx-dependent reductase activities of GvFFTR, CaFFTR2_Gvtail and EcNTR_Gvtail were assessed by estimating the ratio of reduced/oxidized state of Trx (GvTrx-m, CaTrx2 and EcTrx, respectively) in a reaction mixture containing 500 μM NADPH, 1 μM *Anabaena* FNR, 10 μM Fdx1 (or *Anabaena* Flv), 1 μM thioredoxin reductase, and 5 μM Trx in buffer, 50 mM Tris/HCl 7.6, 100 mM NaCl. After 1 h of incubation at room temperature, proteins were precipitated with trichloroacetic acid and resuspended in a solution containing 1 % (*w/v*) SDS and 10 mM 4-acetamido-4′-maleimidylstilbene-2,2′-disulfonic acid (AMS). Samples were subjected to 12 % (w/v) non-reducing SDS-PAGE and visualized with BlueSafe (NZYTech).

2.6. Isothermal titration calorimetry (ITC)

The ITC experiment was performed using an AutoITC200 system (Microcal). Briefly, 20 μM FFTR_W315A in buffer 100 mM potassium phosphate, 2 mM EDTA, pH 7.0 was titrated at 25 °C with a 300 μM Fdx1 solution. The resulting heat changes were integrated and fitted using a single-site binding model implemented in the Origin software package (OriginLab Corporation, Northamptom, MA).

3. Results and discussion

3.1. Trp315 shapes the local flavin environment

To elucidate the specific contribution of Trp315 to the electronic environment of the flavin cofactor in FFTR, we analyzed the absorption and fluorescence spectra of oxidized FFTR_WT ($FFTR\_WT_{ox}$) and selected mutants. The absorption spectra of $FFTR\_WT_{ox}$, the C-terminal truncated variant $FFTR\_\Delta tail_{ox}$ and the $FFTR\_C135S_{ox}$ mutant protein have been previously reported, providing a foundational view of the flavin environment in distinct structural contexts [5,6,11]. Building on this framework, we focus on the $FFTR\_W315A_{ox}$ point mutant protein to assess the specific role of the C-terminal Trp residue (Trp315 in *G. violaceus*) in modulating flavin electronic properties.

Spectroscopic analysis of $FFTR\_W315A_{ox}$ revealed two absorption maxima at 380 nm and 450 nm, corresponding to flavin bands II and I, respectively (Fig. 1B, orange line). These bands were blue-shifted relative to $FFTR\_WT_{ox}$ (Fig. 1B, green line), indicating a perturbed flavin environment. Notably, the spectrum of $FFTR\_W315A_{ox}$ closely resembled that of $FFTR\_\Delta tail_{ox}$ (Fig. 1B, blue line), suggesting that the loss of Trp315—whether by truncation or point mutation—results in similar alteration of the isoalloxazine environment. The similarity between the absorption spectra of free FAD_{ox} (Fig. 1B, purple line) and those of $FFTR\_W315A_{ox}$ and $FFTR\_\Delta tail_{ox}$ likely reflects a comparable solvent-exposed environment of the isoalloxazine *re* face. This convergence supports the hypothesis that disruption of the π-stacking interaction between the aromatic residue and FAD increases solvent exposure of the cofactor. The larger blue shift observed for band II (12 nm) compared to band I (8 nm) reflects their distinct electronic transitions and is consistent with a higher environmental sensitivity of band II. Similar differential shifts in the visible absorption bands of FAD have been reported in other enzymes, such as cholesterol oxidases, where they were attributed to changes in the polarity and hydrophobicity of the active site [28].

Fluorescence measurements upon excitation at 280 nm revealed that $FFTR\_WT_{ox}$ displayed an emission spectrum centered at 333 nm with a shoulder at 352 nm (Fig. 1C, green continuous line). The corresponding excitation spectrum revealed a major peak near 290 nm (Fig. 1C, green dashed line), consistent with the fluorescence characteristics of Trp residues [29]. The emission peak at 333 nm and the shoulder around 352 nm correspond to buried and solvent-exposed Trp side chains, respectively. This interpretation is supported by the structural composition of FFTR, which contains five Trp residues per protomer, two of them buried, two solvent-exposed, and one (Trp315) directly engaged in π-stacking with the FAD isoalloxazine ring (Fig. 1A). In contrast, $FFTR\_\Delta tail_{ox}$ and $FFTR\_W315A_{ox}$ exhibited a marked decreased in Trp fluorescence intensity (Fig. 1C, blue and orange continuous line, respectively), while preserving similar peak-to-shoulder ratios (1.2, 1.1 and 1.1 for WT FFTR, FFTR_Δtail and FFTR_W315A). This pattern confirms that Trp315 contributes significantly to the overall Trp fluorescence signal. The higher fluorescence intensity observed in the WT protein is partly attributable to the presence of this additional Trp residue. However, the fact that Trp315 is π-stacked with the isoalloxazine ring yet still contributes to the emission suggests that this stacking interaction does not lead to complete fluorescence quenching.

Within the flavin fluorescence range, $FFTR\_WT_{ox}$ showed low emission and excitation intensities, consistent with strong quenching of the isoalloxazine fluorescence (Fig. 1D, green colour) [30]. In contrast, both $FFTR\_\Delta tail_{ox}$ and $FFTR\_W315A_{ox}$ displayed an increase in FAD_{ox} fluorescence quantum yield, with $FFTR\_\Delta tail_{ox}$ showing the most pronounced enhancement (Fig. 1D, blue and orange lines). Importantly, the quantum yields of both mutants exceed that of free FAD_{ox} (Fig. 1D, purple line), suggesting that the cofactor remains tightly bound in an extended conformation, lacking the intramolecular folding of the adenine moiety over the isoalloxazine ring that typically contributes to fluorescence quenching in free FAD_{ox} [31]. Thus, the observed increase in fluorescence is not due to cofactor release, but rather to altered interactions within the active site.

These data indicate that in $FFTR\_WT_{ox}$, the FAD is tightly shielded by π–stacking with the Trp315 indole ring, which reduces solvent accessibility and contributes to isoalloxazine fluorescence quenching. Despite the close proximity between Trp315 and the isoalloxazine, no evidence of Förster resonance energy transfer (FRET) from Trp to FAD was observed upon excitation at 280 nm. Furthermore, the strong quenching of FAD fluorescence even upon direct excitation indicates that its lack of emission arises from intrinsic non-radiative decay pathways. Therefore, although no fundamental restriction exists for FRET between Trp and isoalloxazine, the specific geometry and electronic environment in FFTR likely preclude efficient energy transfer.

In contrast, the spectral properties of FFTR_W315A$_{ox}$ and FFTR_Δtail$_{ox}$ resemble those of free FAD$_{ox}$, suggesting that removal of the C-terminal Trp exposes the isoalloxazine ring to a more polar environment, thereby increasing its solvent accessibility. This mirrors the architecture observed in clostridial FFTRs, which naturally lack the C-terminal extension and display fully solvent-exposed FAD cofactors in the resting conformational state [8]. Thus, Trp315 appears to be a structural distinctive feature of cyanobacterial FFTRs that serves the purpose of modulating the flavin environment and, as a consequence, its redox behavior.

3.2. Contributions of the C-terminal tail and Trp315 to FAD redox tuning

The increased solvent accessibility of the isoalloxazine moiety of FAD in FFTR_Δtail and FFTR_W315A compared to FFTR_WT suggests changes in the thermodynamic properties of the FAD cofactor. To test this hypothesis and to quantify the contribution of Trp315 and the C-terminal tail to redox tuning, we determined the midpoint reduction potential of FAD in each variant. Relative to the previously reported $E_{FADox/hq}$ value of −448 ± 8 mV for FFTR_WT (vs. normal hydrogen electrode, NHE) [11], both FFTR_Δtail and FFTR_W315A exhibited significantly less negative values (247 ± 4 mV and −242 ± 4 mV, respectively; Fig. 2A). These results demonstrate that the C-terminal tail, and Trp315 in specifically, plays a critical role in stabilizing the highly negative redox potential of the FAD cofactor in FFTR_WT.

In FFTR_WT, the disulfide potential (−356 mV) lies between those of FAD and canonical Trxs (~−290 mV) [32], establishing a thermodynamically favorable ET sequence from Fdx1 to FAD, then to the disulfide, and finally to Trx [11]. The positive shift in FAD potential observed in the studied mutants disrupts this gradient, reducing the driving force for ET to the disulfide. The disulfide potential is assumed to remain unchanged in FFTR_Δtail and FFTR_W315A, as structural data (PDB codes 5J60 and 6XTF) indicate that the disulfide microenvironment is not directly affected by the removal of Trp315 or the C-terminal tail. Previous observations of partial FAD reoxidation upon Trx addition to DTH-reduced FFTR_Δtail [6] reflect inefficient ET to Trx, likely due to impaired coupling.

Additional insights were obtained from CV measurements. Immobilized FFTR_WT showed no observable redox peaks (Fig. 2B, green line), likely reflecting conformational heterogeneity or insufficient interaction of redox centres with the electrode, whereas FFTR_Δtail and FFTR_W315A each displayed peaks consistent with faster and more homogeneous redox behavior, appearing as a single redox couple (Fig. 2B, blue and orange lines) despite containing two redox-active sites. This observation suggests that the redox window of FAD and disulfide overlaps under the experimental conditions, rendering them electrochemically indistinguishable. The sharper peak definition observed in the mutants likely reflects increased FAD solvent exposure, facilitating more efficient electronic communication with the electrode. Midpoint potentials derived from CV measurements were − 164 ± 5 mV for both mutants (vs. NHE). Considering the known shift in FAD potential upon electrode immobilization (from −219 mV in solution to −135 mV on carbon electrodes; [23,24]), we applied a correction factor to approximate solution-equivalent values. This yielded adjusted midpoint potentials of −244 ± 5 mV for the mutants, in good agreement with the values obtained from potentiometric titrations in solution.

3.3. Modulation of FAD reactivity toward dithionite

To investigate how the C-terminal tail influences the flavin reductive half-reaction in FFTR mutants, we exposed them with DTH, a widely used non-physiological flavin reductant. In previous studies, FFTR_WT required high DTH concentrations to achieve reduction of its FAD cofactor (which holds a very negative redox potential) and, even under these conditions, a mixture of redox species was observed, including the neutral flavin semiquinone (FAD$_{sq}$; one-electron reduced) and the

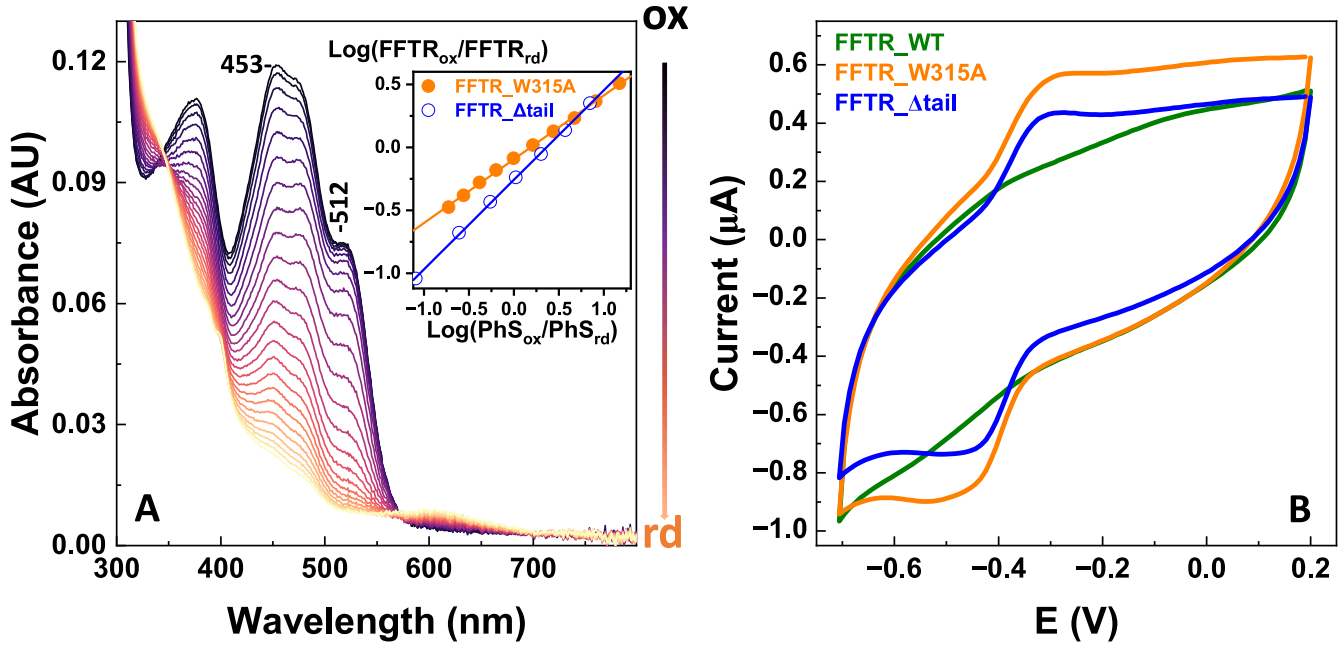

Fig. 2. Midpoint reduction potentials for FFTR_Δtail and FFTR_W315A. A Visible absorption spectra during midpoint reduction potential determination of FFTR_W315A in the presence of phenosafranine as dye (E_m = −252 mV). Spectra from dark-blue to orange represent different time points during protein/dye reduction (right arrow represents direction of changes). Samples were premixed with methyl viologen, xanthine and the dye, rendered anaerobic by several cycles of vacuum application and bubbling with O_2–free argon, and subsequently mixed with xanthine oxidase. Spectra were recorded every 3–5 min for up to 2 h, at 25 °C in 20 mM Tris/HCl pH 8.0, 150 mM NaCl. The inset shows the logarithmic ratios of oxidized/reduced protein (for both FFTR_W315 (orange) and FFTR_Δtail (blue) and dye, with absorption values at 453 nm (flavin band I) and 512 nm (phenosafranine). B Cyclic voltammograms of FFTR_WT (green), FFTR_Δtail (blue), and FFTR_W315A (orange) recorded at 25 °C under anaerobic conditions by applying a potential between 0 and - 700 mV with a scan rate of 100 mV/s. Images shown correspond to a representative of n = 3. (For interpretation of the references to colour in this figure legend, the reader is referred to the web version of this article.)

thiolate-flavin charge transfer complex (CTC) [6,11]. These species indicate incomplete reduction and have been associated with redox asymmetry within the FFTR dimer; that is, while FAD in one monomer proceeded to FAD_{hq} and formed the CTC, the FAD in the other monomer remained as FAD_{ox} or FAD_{sq}. This asymmetry was proposed to regulate electron distribution and reactivity [11].

In striking contrast, FFTR_Δtail and, especially, FFTR_W315A exhibited rapid and complete flavin reduction at much lower DTH concentrations (5 mM versus 50 mM), with negligible accumulation of either FAD_{sq} or CTC (Fig. 3A and B), in agreement with their less negative redox potentials. These observations extend previous findings of enhanced FAD reactivity in the C-terminal truncated variant [6] and further support a central role for Trp315 in modulating the redox properties of FAD, including its intrinsic redox potential and accessibility to external reductants.

Despite the fact that both mutants lack the π-stacking interaction with Trp315, their reduction kinetics by DTH differ. FFTR_Δtail reduction showed two clear kinetically separable processes contributing approximately equally to the total absorbance changes at band I (Fig. 3A, inset), whereas in FFTR_W315A the faster process accounts for only about one quarter of the overall change (Fig. 3B, inset). This suggests that, beyond modulating flavin thermodynamics, the C-terminal tail also imposes kinetic constraints on reductant access. Its complete removal in FFTR_Δtail eliminates this barrier, while substitution of Trp315 in FFTR_W315A only partially relieves it, resulting in an intermediate behavior likely due to partial occupancy of the indole site by the alanine's methyl group.

3.4. Stabilization of catalytic intermediates by the C-terminal tail

To further dissect the mechanistic role of Trp315 and the C-terminal tail, we complemented the chemical reduction assays with light-driven flavin reduction, which offers a more physiologically relevant activation mode and allows detection of transient intermediates. In FFTR_WT, photoreduction generated transient mixtures of FAD_{sq} and CTC, with the FAD_{sq} fraction remaining below 50 % [11].

In contrast, stepwise photoreduction of FFTR_W315A produced a distinct spectral profile that is characterized by a broad band between 550 and 700 nm, with a maximum at 577 nm and a shoulder at 620 nm, along with isosbestic points at 502 and 342 nm (Fig. 4A). This pattern is consistent with partial accumulation of FAD_{sq} (approximately 25 %) and the absence of CTC. These results align with previous data on FFTR_Δtail, which also fails to stabilize FAD_{sq} or form CTC [5].

Stopped-flow photoreduction kinetics in the presence of photosensitizers revealed that both FFTR_Δtail and FFTR_W315A undergo faster and more extensive reduction than FFTR_WT (Fig. 4B and C; [11]), displaying two kinetically distinct reductive processes at band I (Fig. 4B and C, insets). However, despite this increased reactivity, neither mutant achieved full conversion to FAD_{hq}, stabilizing minor long-wavelength intermediates instead (Fig. 4B–C, compare with Fig. 3C in [11]).

These findings indicate that removal of Trp315 destabilizes FAD_{sq}, preventing its progression to FAD_{hq} and abolishing CTC formation. Mechanistically, the observed behavior is consistent with an alteration of the functional asymmetry proposed for the FFTR_WT homodimer—in which one monomer accumulates FAD_{ox}/FAD_{sq} and the other reaches FAD_{hq}/CTC [11]. This reduction in heterogeneity likely reflects a decreased capacity to stabilize distinct intermediate states within the homodimer, which may be critical for efficient coupling of electron donor and acceptor redox centers to the FAD. Taken together, chemical and photoreduction experiments reveal that Trp315 not only modulates the redox potential and accessibility of FAD, but also stabilizes key intermediates and facilitates functional asymmetry within the FFTR dimer. The absence of the C-terminal tail in Clostridium FFTRs may reflect a fundamental difference in their redox requirements. In these enzymes, a single Fdx molecule, containing two [4Fe-4S] redox centers, can subsequently deliver two reducing equivalents to fully convert FAD_{ox} to FAD_{hq}, eliminating the need for stabilization of partially reduced intermediates. By contrast, cyanobacterial FFTRs rely on sequential electron delivery by two [2Fe-2S] Fdx molecules. In this case, stabilization of intermediate FAD_{sq} states is essential to prevent premature reoxidation while awaiting the binding of the second Fdx. Thus, the C-terminal extension in cyanobacterial FFTRs may have evolved to provide structural support for intermediate stabilization, thereby ensuring efficient progression toward complete flavin reduction.

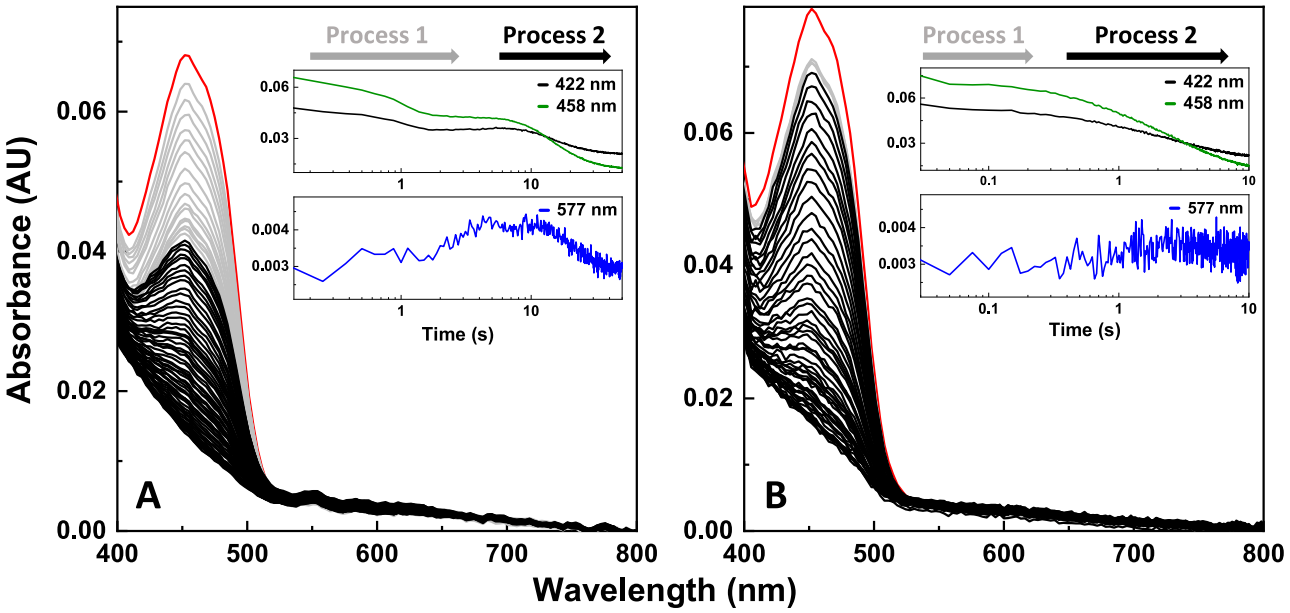

Fig. 3. Time-resolved spectral evolution during reduction of FFTR_Δtail and FFTR_W315A by non-physiological electron donors. Spectral changes observed upon stopped-flow mixing of A FFTR_Δtail (~3.4 μM, homodimer concentration) and B FFTR_W315A (~3.1 μM) with 5 mM DTH. Insets show kinetic traces at representative wavelengths. Major processes are indicated by grey (first process) and black (second process) spectra with arrows. In all panels, the red line corresponds to the first spectrum after mixing. Reactions were performed under anaerobic conditions at 25 °C in 20 mM Tris/HCl (pH 8.0), 150 mM KCl. Data correspond to a representative experiment ($n > 3$). (For interpretation of the references to colour in this figure legend, the reader is referred to the web version of this article.)

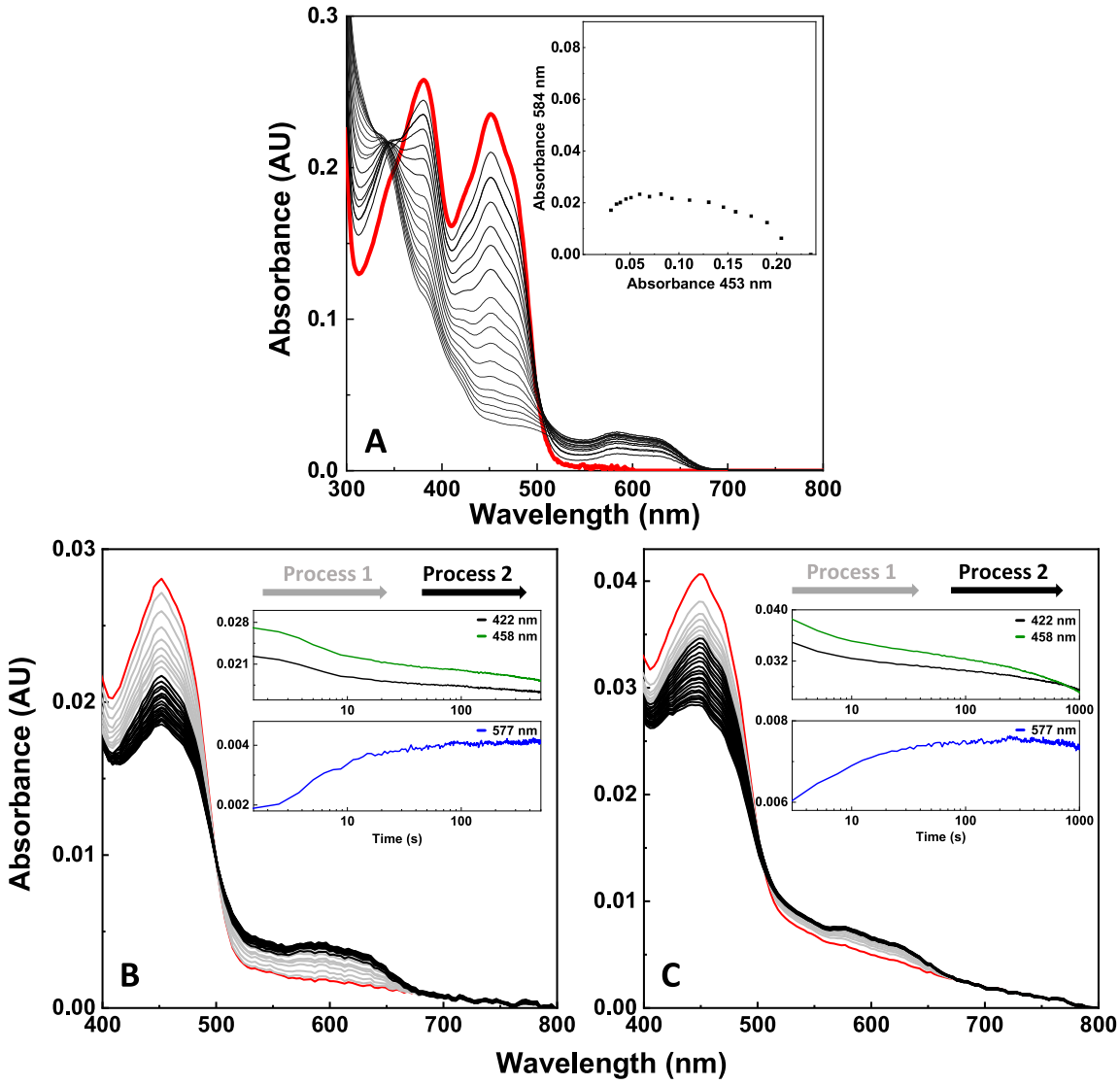

Fig. 4. Light-driven flavin reduction in FFTR mutants. A Spectral evolution during steady-state photoreduction of FFTR_W315A (~9 μM homodimer). The inset shows the absorbance at the FAD neutral semiquinone band maximum (584 nm) relative to flavin band I maximum (450 nm). Photoreductions were performed under anaerobiosis with 4 μM 5-dRf and 3 mM EDTA. Spectral changes elicited by the stopped-flow light source upon mixing of buffer with B FFTR_Δtail (~1.1 μM, homodimer) or C FFTR_W315A (~1.3 μM, homodimer). Insets display kinetic traces at representative wavelengths, following maxima of $Fdx1_{ox}$, band-I of FAD_{ox} and band of FAD_{sq}. Major identified processes are indicated by grey (first) and black (second), with corresponding arrows in the insets. The initial oxidized state in A and the first spectrum after mixing in B and C are shown in red. All measurements were performed in 20 mM Tris/HCl, 150 mM KCl, pH 8.0 under anaerobic conditions at 25 °C, and stopped-flow experiments contained 1.5 mM EDTA and 2 μM 5-dRf final concentrations. Images shown correspond to a representative of $n > 3$. (For interpretation of the references to colour in this figure legend, the reader is referred to the web version of this article.)

3.5. Role of the C-terminal tail and Trp315 in donor recognition

The C-terminal tail of FFTR plays a key role in mediating interactions with Fdx1, enabling efficient ET through the FAD to the redox-active disulfide, as previously demonstrated by X-ray crystallography, ITC, and biochemical assays that confirmed specific binding and catalytic activity [5,6,11].

To test the contribution of the π-stacking interaction to donor recognition, we performed ITC experiments using the FFTR_W315A mutant. Titration with oxidized Fdx1 ($Fdx1_{ox}$) produced no measurable heat change (Fig. 5A), indicating a lack of specific binding. These results suggest that disruption of the π-stacking interaction may be sufficient to impair functional docking with Fdx1. Although the C-terminal tail is still present in FFTR_W315A, it may be destabilized in the absence of Trp315, compromising its ability to mediate productive donor interaction. Thus, the π-stacking interaction between Trp315 and the FAD cofactor is not merely a local electronic feature, but also contributes to maintaining the structural integrity of the donor-binding interface.

Consistent with the unfavorable redox potential of FAD, neither FFTR_W315A nor FFTR_Δtail mutants supported disulfide reduction by DTNB in the presence of reduced Fdx1, with or without Trx (Fig. 5B). These findings indicate that ET from Fdx1 to the disulfide is severely hindered in both mutants, suggesting a loss of functional coupling due either to impaired donor docking or to insufficient thermodynamic driving force.

To further evaluate the donor specificity of FFTR, we tested whether the enzyme could accommodate Flv, a structurally distinct yet functionally analogous one-electron carrier that substitutes for Fdx in various redox pathways [33]. Unlike plant-type Fdx, which contains a [2Fe—2S] cluster, Flv carries a flavin mononucleotide (FMN) cofactor and operates via the FMN_{sq}/FMN_{hq} redox pair. Despite their structural differences, both proteins act as low-potential one-electron carriers (−400 to −430 mV) [34,35]. Activity assays using reduced *Anabaena* Flv confirmed that *Gloeobacter* FFTR_WT can efficiently use Flv to support

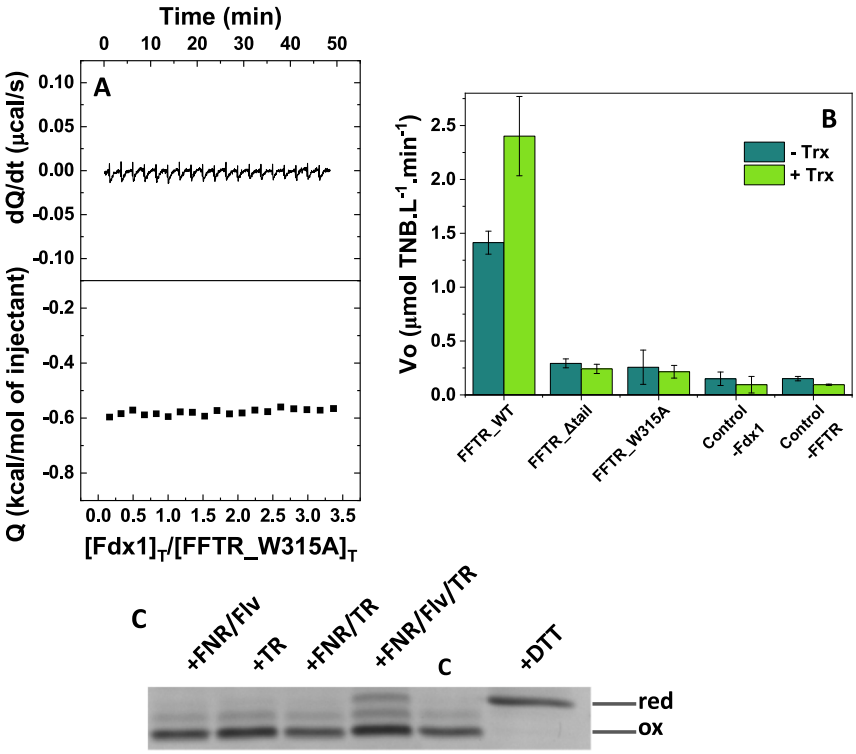

Fig. 5. FFTR_Δtail and FFTR_W315A in the electron transfer pathway from Fdx1 to the disulfide active site. A ITC analysis of the interaction between *G. violaceus* Fdx1 and FFTR_W315A. The upper plot shows the thermograms of heat release upon sequential Fdx1 injections to the FFTR_W315A protein solution. The lower panel shows the binding isotherm (Fdx-normalized integrated heats per injection as a function of the molar ratio $[Fdx1]_{Total}/[FFTR\_W115A]_{Total}$). B DTNB reduction assay of FFTR_WT, FFTR_Δtail, and FFTR_W315A using Fdx1 as electron donor, in the absence (−Trx) or presence (+Trx) of Trx-m. DTNB reduction was followed at 412 nm; initial velocities calculated. Controls lacking Fdx1 (–Fdx1) or FFTR (–FFTR) are included. Data are mean ± SD. C Flv-dependent reduction of *G. violaceus* Trx-m via *G. violaceus* FFTR with *Anabaena* Flv reduced by *Anabaena* FNR in the presence of NADPH. The reaction mixture contained equal amounts of Trx-m, NADPH, and components as indicated. After reaction, free thiols in Trx-m were labeled with AMS, shifting its electrophoretic mobility. Oxidized (C, control) and reduced (DTT-treated) Trx-m are included for comparison.

Trx reduction (Fig. 5C). This result indicates that, despite the strict structural requirements observed for the specific interaction with Fdx1, the FFTR_WT active site retains a degree of flexibility that allows engagement with alternative redox partners. Such adaptability may be physiologically relevant in environments where Fdx availability is limited, such as iron-poor conditions, underscoring the capacity of FFTR_WT to integrate diverse electron input systems.

3.6. Electron transfer from $Fdx1_{rd}$ to FFTR mutants in the absence of specific docking

To evaluate whether the FAD cofactors in FFTR_Δtail and FFTR_W315A retain the ability to accept electrons from reduced Fdx1 ($Fdx1_{rd}$), we monitored flavin reduction upon mixing photoreduced $Fdx1_{rd}$ with each FFTR mutant (Fig. 6). This experiment does not assess specific protein–protein interaction, as both mutants lack the C-terminal tail required for Fdx1 docking, as demonstrated above (Fig. 5A–B). Instead, it probes the intrinsic capacity of the solvent- exposed FAD cofactors to undergo reduction under solution-phase conditions, where ET may occur via transient collisions, following the approach previously established for FFTR_WT (see Fig. 4-B in [11]).

Spectral analysis revealed that both FFTR variants underwent complete reduction to the FAD_{hq} state at [2Fe—2S]:FAD ratios of 1:2 and 4:2 (Fig. 6A–D). At the highest ratio, sufficient electrons were available to reduce both FAD cofactors within the homodimer. Notably, FFTR_W315A exhibited two distinct kinetic phases during reduction (Fig. 6D, inset), consistent with asynchronous reduction of the two monomers—similar to the behavior previously observed for FFTR_WT [11]. In contrast, FFTR_Δtail displayed a single kinetic phase, suggesting simultaneous reduction of both monomers (Fig. 6B). Both mutants achieved the FAD_{hq} state significantly faster than FFTR_WT under identical conditions. This enhanced reactivity likely reflects their less negative FAD midpoint potentials, which lower the energetic barrier for reduction.

FFTR_WT can reach a final dithiol-FAD_{hq} (EH_4) state during the evaluated process, as subsequent photoreduced $Fdx1_{rd}$ molecules facilitate a second FAD reduction cycle following reoxidation via hydride transfer to the redox-active disulfide. In contrast, this outcome is not expected for the mutants, owing to their inability to reduce the disulfide bridge (Fig. 5B). Consequently, the final state in the mutants is expected to be the disulfide-FAD_{hq}.

These results demonstrate that although FAD in FFTR_Δtail and FFTR_W315A can still accept electrons from $Fdx1_{rd}$, the variants lack the environment required to stabilize a sufficiently negative midpoint potential and to support efficient intramolecular ET to the redox-active disulfide. As shown above, alterations in the C-terminal tail may also impair proper docking of Fdx1 to the enzyme. Altogether, our findings reveal that the C-terminal tail fulfils a dual role: it establishes a productive donor-binding interface while simultaneously shaping the FAD environment to meet the thermodynamic and kinetic requirements for efficient intramolecular ET.

3.7. Functional integration of the FFTR C-terminal tail requires structural context

Building on the observation that Trp315 modulates flavin redox properties through π-stacking interactions, we asked whether this structural element could be introduced into other flavoproteins to confer

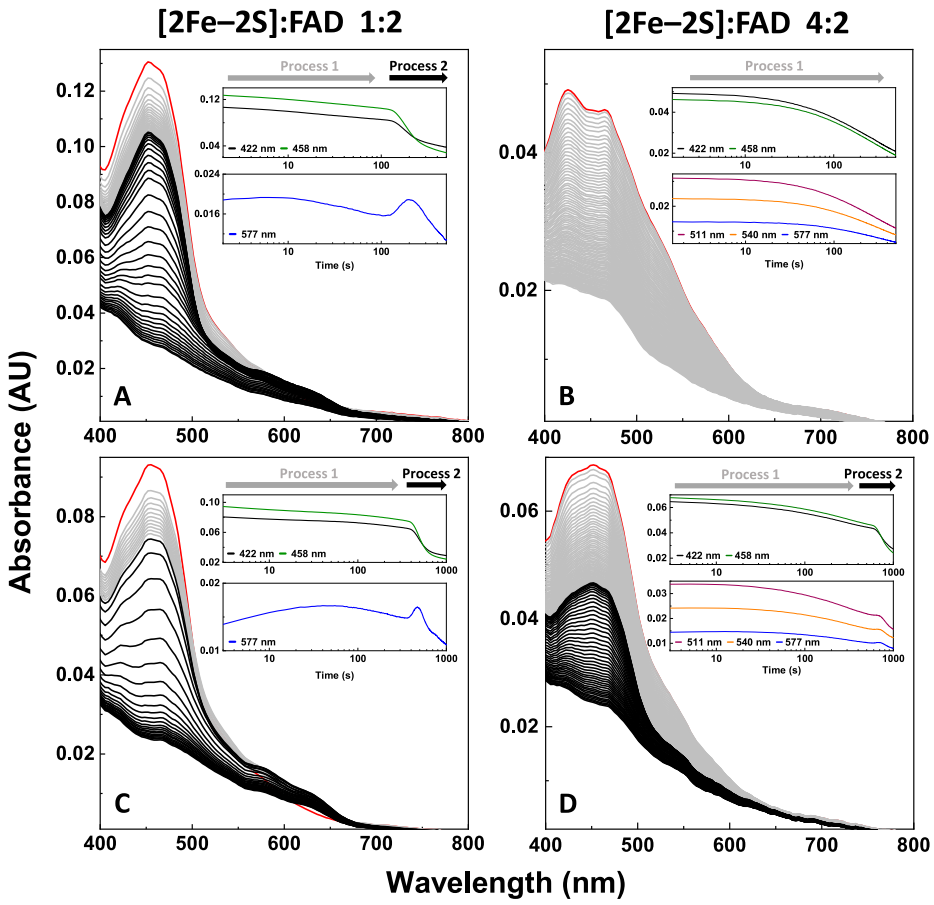

Fig. 6. Fdx1 as electron donor to the FAD cofactor in FFTR_Δtail and FFTR_W315A. Spectral evolution observed upon mixing $Fdx1_{rd}$ with the FFTR_$Δtail_{ox}$ homodimer at [2Fe—2S]:FAD ratios of A 1:2 and B 4:2, and with FFTR_$W315A_{ox}$ at [2Fe—2S]:FAD ratios of C 1:2 and D 4:2, recorded by stopped-flow spectroscopy under anaerobic conditions. Insets show kinetic traces at representative wavelengths, following maxima of $Fdx1_{ox}$, band-I FAD_{ox} and neutral FAD_{sq}. In all panels, the first spectrum after mixing is shown in red. Major identified processes are highlighted by grey (first) and black (second) spectra, respectively, as well as by arrows of the same colour in the insets. All measurements were performed in 20 mM Tris/HCl, 150 mM KCl, pH 8.0 under anaerobic conditions at 25 °C, and contained 1.5 mM EDTA and 2 μM 5-dRf. Images shown correspond to a representative of n > 3. (For interpretation of the references to colour in this figure legend, the reader is referred to the web version of this article.)

similar functionality. This question is particularly relevant because stabilization of the FAD_{sq} intermediate could, in principle, enable sequential single-ET. In most Fdx-dependent systems, partner recognition is primarily governed by electrostatic complementarity, allowing a degree of cross-species compatibility. Crystallographic analysis has further shown that the C-terminal tail of *Gloeobacter* FFTR directly participates in Fdx1 binding (PDB 6XTF).

To test the contribution of the tail to functional flexibility, we engineered two chimeric constructs. In the first construct, the C-terminal segment of *Gloeobacter* FFTR was fused to clostridial FFTR (CaFFTR2_Gvtail), which naturally lacks a tail and operates with Fdxs containing two [4Fe–4S] clusters, thereby donating two electrons sequentially. This chimera showed no detectable activity with cyanobacterial [2Fe—2S] Fdx1 (Fig. 7A), indicating that the tail alone may be insufficient to enable productive coupling with one-electron donors, and that additional structural determinants are likely required to stabilize FAD_{sq} and support ET. In a second construct, the *Gloeobacter* tail was appended to *E. coli* NTR (EcNTR_Gvtail), a flavoprotein in which domain rotation enables FAD to shuttle electrons between NADPH and the disulfide active site [9]. EcNTR_Gvtail retained NADPH-dependent activity (Fig. 7B), demonstrating that the inserted tail is structurally compatible and does not interfere with cofactor binding or the native redox mechanism. Although weak interactions between free Trp and FAD have been reported in solution [36], the structural constraints of the protein matrix appear crucial for stabilizing this interaction in a catalytically relevant configuration.

Together, these experiments highlight that the functional role of the C-terminal tail is intrinsically linked to its structural context. Rather than acting as a modular element, its ability to support redox partner interactions and tune FAD reactivity depends on precise spatial and dynamic features, underscoring the co-evolution of redox motifs with their protein environments across flavoprotein families.

4. Conclusions

Our study demonstrates that the π-stacking interaction between Trp315 and the FAD isoalloxazine ring is a central determinant of FFTR redox behavior. Disruption of this interaction—through C-terminal tail truncation or Trp mutation—destabilizes the flavin, increases its solvent exposure, and shifts its redox potential by ~200 mV, thereby impairing ET to the redox-active disulfide.

Spectroscopic and kinetic analyses reveal that both FFTR_W315A and FFTR_Δtail adopt an open conformation reminiscent of clostridial FFTRs, indicative of a conserved resting state. In cyanobacteria, the C-terminal tail stabilizes FAD_{sq}, imposes structural gating, and modulates ET both within and between protomers. Mutants lacking the tail exhibit more synchronized reduction, highlighting its role in dynamic asymmetry.

Chimeric experiments demonstrate that the tail is not a modular element, but instead requires precise structural and electronic

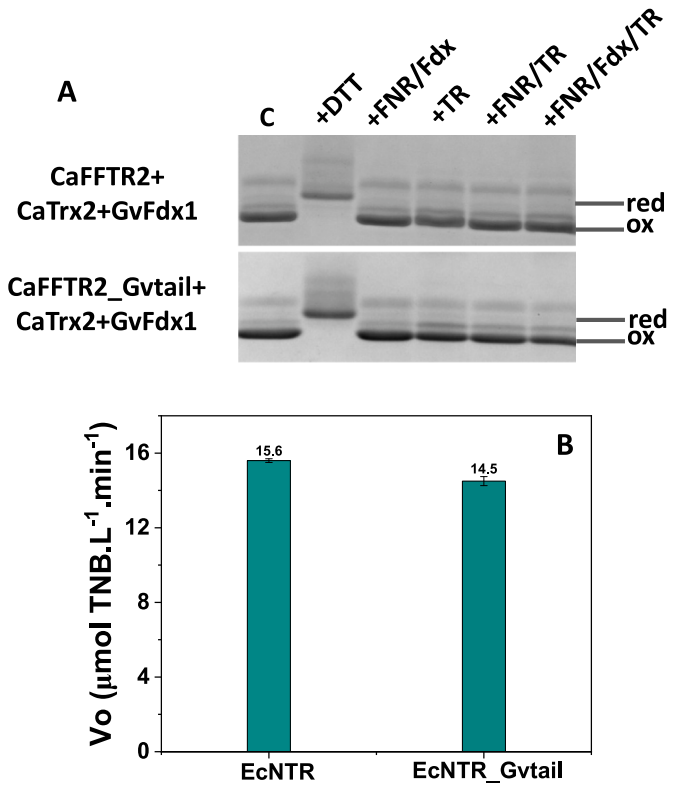

Fig. 7. Activity of thioredoxin reductase chimeras. A Reduction of CaTrx2 via CaFFTR2 and CaFFTR2_Gvtail with electrons derived from *G. violaceus* [2Fe-2S] Fdx1, reduced by *Anabaena* FNR in the presence of NADPH. Reaction mixtures contained equal amounts of Trx, NADPH, and components as indicated, with TR referring to the corresponding FFTR version. After reaction, free sulfhydryl groups were labeled with AMS, which increases the mass of the protein by about 0.5 KDa per free thiol, allowing the two different redox states of CaFFTR2 (reduced or oxidized) to be separated by SDS-PAGE under nonreducing conditions. CaTrx2 in the oxidized state (C, control) and in the reduced state (after DTT incubation) are included for comparison. B NADPH-dependent thioredoxin reductase activity of EcNTR and EcNTR_Gvtail. The reduction of DTNB to TNB was monitored as an increase in absorbance at 412 nm, and the initial velocity was calculated (expressed as µmol $TNB{\cdot}L^{-1}{\cdot}cm^{-1}{\cdot}min^{-1}$). Reactions were performed in 100 mM potassium phosphate buffer, pH 7.0, containing 2 mM EDTA, 0.15 mM NADPH, 0.25 µM NTR (EcNTR or EcNTR_Gvtail), and 0.25 mM DTNB at 25.
°C. Bars represent mean values ± SD from three independent experiments.

compatibility with native partners, consistent with co-evolution. The ability of *Gloeobacter* FFTR to utilize Flv further highlights its adaptation to single-ET and the physiological relevance of FAD_{sq} stabilization.

Altogether, these findings establish FFTR as a model system for redox modulation through dynamic structural features, providing insights for the engineering of flavoproteins with tailored redox properties.

CRediT authorship contribution statement

Martha Minjarez-Saenz: Investigation, Formal analysis. **Víctor Correa-Pérez:** Investigation, Formal analysis. **Maribel Rivero:** Investigation, Formal analysis. **Sheila J. Sadeghi:** Investigation, Formal analysis. **Javier Calvo:** Investigation. **Adrián Velázquez-Campoy:** Investigation, Formal analysis. **Federico Gago:** Writing – review & editing, Methodology. **Rubén M. Buey:** Writing – review & editing, Formal analysis. **Marta Martínez-Júlvez:** Writing – review & editing, Formal analysis. **Milagros Medina:** Writing – original draft, Visualization, Supervision, Project administration, Investigation, Funding acquisition, Formal analysis, Conceptualization. **Monica Balsera:** Writing – original draft, Validation, Supervision, Project administration, Investigation, Funding acquisition, Formal analysis, Conceptualization.

Declaration of competing interest

The authors declare no conflicts of interest.

Acknowledgements

We thank David García López for excellent technical assistance, as well as the Servicios Generales de Apoyo a la Investigación-SAI, Universidad de Zaragoza and the DNA Sequencing Service (NUCLEUS), University of Salamanca, for their technical support. This work was supported by the Spanish State Research Agency and FEDER (MCIN/AEI-FEDER) (Grants numbers PID2022-136369NB-I00, PID2019-110900GB-I00, PID2023-150714OB-I00 and PID2022-136307OB-C22), as well as the Government of Aragón-FEDER (Grant E35_23R).

Data availability

Data will be made available on request.

References

[1] M. Balsera, B.B. Buchanan, Evolution of the thioredoxin system as a step enabling adaptation to oxidative stress, Free Radic. Biol. Med. 140 (2019) 28–35, https://doi.org/10.1016/j.freeradbiomed.2019.03.003.
[2] A. Holmgren, Thioredoxin and glutaredoxin systems, J. Biol. Chem. 264 (1989) 13963–13966.
[3] B.B. Buchanan, Regulation of CO2 assimilation in oxygenic photosynthesis: the ferredoxin/thioredoxin system, Arch. Biochem. Biophys. 288 (1991) 1–9, https://doi.org/10.1016/0003-9861(91)90157-e.
[4] K.E. Hammel, K.L. Cornwell, B.B. Buchanan, Ferredoxin/flavoprotein-linked pathway for the reduction of thioredoxin, Proc. Natl. Acad. Sci. USA 80 (1983) 3681–3685, https://doi.org/10.1073/pnas.80.12.3681.
[5] R.M. Buey, D. Fernández-Justel, G. González-Holgado, M. Martínez-Júlvez, A. González-López, A. Velázquez-Campoy, M. Medina, B.B. Buchanan, M. Balsera, Unexpected diversity of ferredoxin-dependent thioredoxin reductases in cyanobacteria, Plant Physiol. 186 (2021) 285–296, https://doi.org/10.1093/plphys/kiab072.
[6] R.M. Buey, S. Galindo-Trigo, L. López-Maury, A. Velázquez-Campoy, J.L. Revuelta, F.J. Florencio, J.M. de Pereda, P. Schürmann, B.B. Buchanan, M. Balsera, A new member of the thioredoxin reductase family from early oxygenic photosynthetic organisms, Mol. Plant 10 (2017) 212–215, https://doi.org/10.1016/j.molp.2016.06.019.
[7] C. Anjou, A. Lotoux, A. Zhukova, M. Royer, L.C. Caulat, E. Capuzzo, C. Morvan, I. Martin-Verstraete, The multiplicity of thioredoxin systems meets the specific lifestyles of *Clostridia*, PLoS Pathog. 20 (2024) e1012001, https://doi.org/10.1371/journal.ppat.1012001.
[8] R.M. Buey, D. Fernández-Justel, J.M. de Pereda, J.L. Revuelta, P. Schürmann, B. B. Buchanan, M. Balsera, Ferredoxin-linked flavoenzyme defines a family of pyridine nucleotide-independent thioredoxin reductases, Proc. Natl. Acad. Sci. USA 115 (2018) 12967–12972, https://doi.org/10.1073/pnas.1812781115.
[9] B.W. Lennon, C.H. Williams, M.L. Ludwig, Twists in catalysis: alternating conformations of *Escherichia coli* thioredoxin reductase, Science 289 (2000) 1190–1194, https://doi.org/10.1126/science.289.5482.1190.
[10] C.H. Williams, L.D. Arscott, S. Müller, B.W. Lennon, M.L. Ludwig, P.F. Wang, D. M. Veine, K. Becker, R.H. Schirmer, Thioredoxin reductase two modes of catalysis have evolved, Eur. J. Biochem. 267 (2000) 6110–6117, https://doi.org/10.1046/j.1432-1327.2000.01702.x.
[11] M. Minjarez-Saenz, V. Correa-Pérez, M. Rivero, A. Hernández-Gómez, M. Martínez-Júlvez, R.M. Buey, F. Gago, M. Balsera, M. Medina, Mechanism of cyanobacterial ferredoxin-dependent flavin thioredoxin reductase reveals thiolate-FAD charge transfer and catalytic asymmetry in a homodimer, FEBS J. (2025), https://doi.org/10.1111/febs.70210.
[12] M. Tanaka, T. Nakashima, A. Benson, H. Mower, K.T. Tasunobu, The amino acid sequence of Clostridium pasteurianum ferredoxin, Biochemistry 5 (1966) 1666–1681, https://doi.org/10.1021/bi00869a032.
[13] N. Muraki, D. Seo, T. Shiba, T. Sakurai, G. Kurisu, Asymmetric dimeric structure of ferredoxin-NAD(P)+ oxidoreductase from the green sulfur bacterium *Chlorobaculum tepidum*: implications for binding ferredoxin and NADP+, J. Mol. Biol. 401 (2010) 403–414, doi:S0022-2836(10)00640-6 [pii], https://doi.org/10.1016/j.jmb.2010.06.024.
[14] I. Lans, M. Medina, E. Rosta, G. Hummer, M. Garcia-Viloca, J.M. Lluch, À. González-Lafont, Theoretical study of the mechanism of the hydride transfer between ferredoxin-NADP+ reductase and NADP+: the role of Tyr303, J. Am. Chem. Soc. 134 (2012) 20544–20553, https://doi.org/10.1021/ja310331v.
[15] I. Lans, J.R. Peregrina, M. Medina, M. García-Viloca, A. González-Lafont, J. M. Lluch, Mechanism of the hydride transfer between Anabaena Tyr303Ser FNRrd/FNRox and NADP+/H. A combined pre-steady-state kinetic/ensemble-averaged

transition-state theory with multidimensional tunneling study, J. Phys. Chem. B 114 (2010) 3368–3379, https://doi.org/10.1021/jp912034m.
[16] S. Frago, G. Goñi, B. Herguedas, J.R. Peregrina, A. Serrano, I. Pérez-Dorado, R. Molina, C. Gómez-Moreno, J.A. Hermoso, M. Martínez-Júlvez, S.G. Mayhew, M. Medina, Tuning of the FMN binding and oxido-reduction properties by neighboring side chains in Anabaena flavodoxin, Arch. Biochem. Biophys. 467 (2007) 206–217. S0003-9861(07)00417-1 [pii], https://doi.org/10.1016/j.abb.2007.08.024.
[17] P.A. Hubbard, C. Xia, A.L. Shen, J.P. Kim, Structural and kinetic investigations of the carboxy terminus of NADPH-cytochrome P450 oxidoreductase, Arch. Biochem. Biophys. 701 (2021) 108792, https://doi.org/10.1016/j.abb.2021.108792.
[18] I. Nogués, J. Tejero, J.K. Hurley, D. Paladini, S. Frago, G. Tollin, S.G. Mayhew, C. Gómez-Moreno, E.A. Ceccarelli, N. Carrillo, M. Medina, Role of the C-terminal tyrosine of ferredoxin-nicotinamide adenine dinucleotide phosphate reductase in the electron transfer processes with its protein partners ferredoxin and flavodoxin, Biochemistry 43 (2004) 6127–6137, https://doi.org/10.1021/bi049858h.
[19] J. Li, C. Li, W. Xiao, D. Yuan, G. Wan, L. Ma, Site-directed mutagenesis by combination of homologous recombination and DpnI digestion of the plasmid template in *Escherichia coli*, Anal. Biochem. 373 (2008) 389–391, https://doi.org/10.1016/j.ab.2007.10.034.
[20] C. Gómez-Moreno, M.-J. M., M.F. Fillat, J.K. Hurley, G. Tollin, Molecular recognition in electron transfer proteins, in: Photosynthesis: From Light to Biosphere Kluwer, Academic Publishers, The Netherlands, 1995, pp. 627–632.
[21] M.F. Fillat, W.E. Borrias, P.J. Weisbeek, Isolation and overexpression in Escherichia coli of the flavodoxin gene from Anabaena PCC 7119, Biochem. J. 280 (Pt 1) (1991) 187–191, https://doi.org/10.1042/bj2800187.
[22] P. Macheroux, UV-visible spectroscopy as a tool to study flavoproteins, Methods Mol. Biol. 131 (1999) 1–7, doi:1-59259-266-X-1 [pii], https://doi.org/10.1385/1-59259-266-X:1.
[23] E. Maklashina, G. Cecchini, Determination of flavin potential in proteins by xanthine/xanthine oxidase method, Bio-Protoc. 10 (2020) e3571, https://doi.org/10.21769/BioProtoc.3571.
[24] S.L. Christgen, S.M. Becker, D.F. Becker, Methods for determining the reduction potentials of flavin enzymes, Methods Enzymol. 620 (2019) 1–25, https://doi.org/10.1016/bs.mie.2019.03.004.
[25] H. Cheropkina, G. Catucci, F. Cesano, A. Marucco, G. Gilardi, S.J. Sadeghi, Bioelectrochemical platform with human monooxygenases: FMO1 and CYP3A4 tandem reactions with phorate, Bioelectrochemistry 150 (2023) 108327, https://doi.org/10.1016/j.bioelechem.2022.108327.
[26] P. Ferreira, M. Medina, Anaerobic stopped-flow spectrophotometry with photodiode array detection in the presteady state: an application to elucidate oxidoreduction mechanisms in flavoproteins, Methods Mol. Biol. 2280 (2021) 135–155, https://doi.org/10.1007/978-1-0716-1286-6_9.
[27] A. Holmgren, M. Björnstedt, Thioredoxin and thioredoxin reductase, Methods Enzymol. 252 (1995) 199–208, https://doi.org/10.1016/0076-6879(95)52023-6.
[28] A. Vrielink, S. Ghisla, Cholesterol oxidase: biochemistry and structural features, FEBS J. 276 (2009) 6826–6843, https://doi.org/10.1111/j.1742-4658.2009.07377.x.
[29] J.R. Lakowicz, Principles of Fluorescence Spectroscopy, 2 ed., Springer, New York, NY, 1999.
[30] J. Galbán, I. Sanz-Vicente, J. Navarro, S. de Marcos, The intrinsic fluorescence of FAD and its application in analytical chemistry: a review, Methods Appl. Fluoresc. 4 (2016) 042005, https://doi.org/10.1088/2050-6120/4/4/042005.
[31] D. Volkov, I. Gorbunova, D. Yashkov, M. Sasin, M. Khrenova, O. Vasyutinskii, The role of conformation states in the heterogeneity of fluorescence decay times in FAD in water–alcohol mixtures, J. Photochem. Photobiol. A Chem. 461 (2025) 1–12, https://doi.org/10.1016/j.jphotochem.2024.116155.
[32] P. Schürmann, B.B. Buchanan, The ferredoxin/thioredoxin system of oxygenic photosynthesis, Antioxid. Redox Signal. 10 (2008) 1235–1274, https://doi.org/10.1089/ars.2007.1931.
[33] A.F. Lodeyro, R.D. Ceccoli, J.J. Pierella Karlusich, N. Carrillo, The importance of flavodoxin for environmental stress tolerance in photosynthetic microorganisms and transgenic plants. Mechanism, evolution and biotechnological potential, FEBS Lett. 586 (2012) 2917–2924, https://doi.org/10.1016/j.febslet.2012.07.026.
[34] M. Medina, Structural and mechanistic aspects of flavoproteins: photosynthetic electron transfer from photosystem I to NADP+, FEBS J. 276 (2009) 3942–3958, doi:EJB7122 [pii], https://doi.org/10.1111/j.1742-4658.2009.07122.x.
[35] G. Goni, B. Herguedas, M. Hervas, J.R. Peregrina, M.A. De la Rosa, C. Gomez-Moreno, J.A. Navarro, J.A. Hermoso, M. Martinez-Julvez, M. Medina, Flavodoxin: a compromise between efficiency and versatility in the electron transfer from photosystem I to ferredoxin-NADP(+) reductase, BBA-Bioenergetics 1787 (2009) 144–154, https://doi.org/10.1016/j.bbabio.2008.12.006.
[36] C.L. Chatterjee, A. Torstensson, C.K. Mitra, 435 — interaction of FAD and NAD with aromatic amino acids, Bioelectrochem. Bioenerg. 81 (1981) 569–574, https://doi.org/10.1016/0302-4598(81)80027-X.